THE JOURNAL OF PHYSICAL CHEMISTRY Letters

Letter

Cite This: J. Phys. Chem. Lett. 2019, 10, 4987−4993

pubs.acs.org/JPCL

Monolayer Modification of VTe_2 and Its Charge Density Wave

Paula Mariel Coelho,[†] Kinga Lasek,[†] Kien Nguyen Cong,[†] Jingfeng Li,[†] Wei Niu,[‡,§] Wenqing Liu,[‡] Ivan I. Oleynik,[†] and Matthias Batzill*[,†]

[†]Department of Physics, University of South Florida, Tampa, Florida 33620, United States

[‡]Department of Electronic Engineering, Royal Holloway University of London, Egham TW20 0EX, U.K.

[§]New Energy Technology Engineering Laboratory of Jiangsu Provence and School of Science, Nanjing University of Posts and Telecommunications, Nanjing 210023, China

Supporting Information

ABSTRACT: Interlayer interactions in layered transition metal dichalcogenides are known to be important for describing their electronic properties. Here, we demonstrate that the absence of interlayer coupling in monolayer VTe_2 also causes their structural modification from a distorted 1T′ structure in bulk and multilayer samples to a hexagonal 1T structure in the monolayer. X-ray photoemission spectroscopy indicates that this structural transition is associated with electron transfer from the vanadium d bands to the tellurium atoms for the monolayer. This charge transfer may reduce the in-plane d orbital hybridization and thus favor the undistorted 1T structure. Phonon-dispersion calculations show that, in contrast to the 1T′ structure, the 1T structure exhibits imaginary phonon modes that lead to a charge density wave (CDW) instability, which is also observed by low-temperature scanning tunneling microscopy as a 4 × 4 periodic lattice distortion. Thus, this work demonstrates a novel CDW material, whose properties are tuned by interlayer interactions.

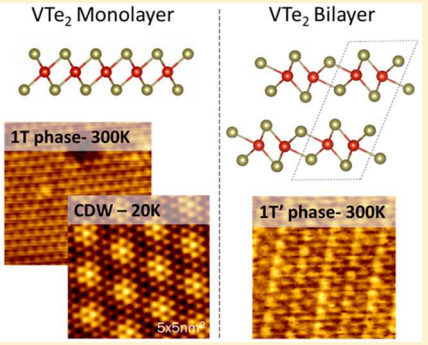

Modifying the properties of materials by controlling interlayer interactions in van der Waals materials is a promising approach for designing new materials and devices. The excitement for this scheme has been fueled by significant findings in interlayer interaction-dependent properties in transition metal dichalcogenides (TMDCs). Examples of modifications of the properties of materials by tuning of interlayer interactions are (i) the indirect-to-direct band gap transition in the group VI dichalcogenide family when interlayer interactions are removed,[1−3] (ii) the strong band gap tunability in noble metal dichalcogenides as a function of layers due to interlayer hybridization,[4−6] (iii) the tunability of the charge density wave transition in $TiSe_2$,[7,8] and $TiTe_2$,[9] and (iv) the recent discovery of a larger Mott insulating state and unique orbital texture in monolayer $TaSe_2$ compared to multilayers.[10] Here, we investigate for the first time layer-dependent structural modifications in TMDCs on the example of VTe_2. In addition to transforming into a simple 1T structure in the monolayer limit, the lack of interlayer interactions also gives rise to a new charge density wave (CDW) material.

Previous studies of monolayers were primarily performed on the hexagonal, high-symmetry 1T (octahedral) or 2H (trigonal prismatic) polymorphs of TMDCs. In contrast, the group V tellurides form a distorted 1T″ structure, known as the ribbon structure,[11−14] which may be described by a double zigzag row (or ribbon) of coordinated transition metals, in a variation of the possibly better-known single zigzag row 1T′ structure (e.g., observed in WTe_2 or β-$MoTe_2$). Illustrations of these three related structures can be found below. The commonality of the distorted variations of the 1T structures is that the length of the bond between some transition metals (TM) is reduced as a consequence of interatomic bonding. The basal plane of the ribbon structure can be described as a 3 × 1 reconstruction and the zigzag structure as a 2 × 1 reconstruction of a hexagonal mesh.[15] The distorted 1T structures, either as a ribbon or a zigzag structure, are understood to arise from in-plane metal coordination through d orbital hybridization. The t_{2g} orbitals in the octahedral 1T structure are split by the lattice distortion in the 1T′ and 1T″ structures and causes a decrease in the energy of the occupied d_{xz} and d_{xy} bonding orbitals. This is possible if the bonding orbitals are each occupied by two electrons (i.e., a total of four). In the ribbon structure, the bonding orbitals are being shared among three TMs thus requiring an electron count of 4/3 d electrons per TM atom.[11] In contrast, a zigzag 1T′ structure would share these orbitals between two TMs and thus requiring an electron count of two d electrons per atom for its formation.[16] These arguments suggest that the structure can be controlled by charge donation and withdrawal from the d orbitals. Interlayer interactions in group V ditellurides have been proposed to be important in determining the d orbital occupancy. Theoretical calculations have shown that Te−Te interlayer coupling raises the Te 5p

Received: July 5, 2019
Accepted: August 14, 2019
Published: August 14, 2019

DOI: 10.1021/acs.jpclett.9b01949
J. Phys. Chem. Lett. 2019, 10, 4987−4993

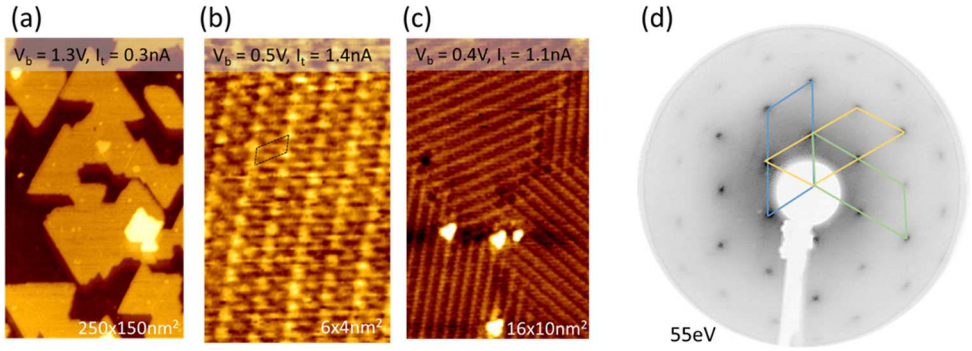

Figure 1. Characterization of multilayer MBE-grown VTe_2. (a) Large scale STM image showing bi- and trilayer terraces. Atomic-resolution images of (b) a 2 × 1 domain and (c) a region showing the coexistence of the three equivalent 2 × 1 domains. The LEED pattern of the sample is shown in panel d with the three reciprocal unit cells of the coexisting 2 × 1 domains indicated.

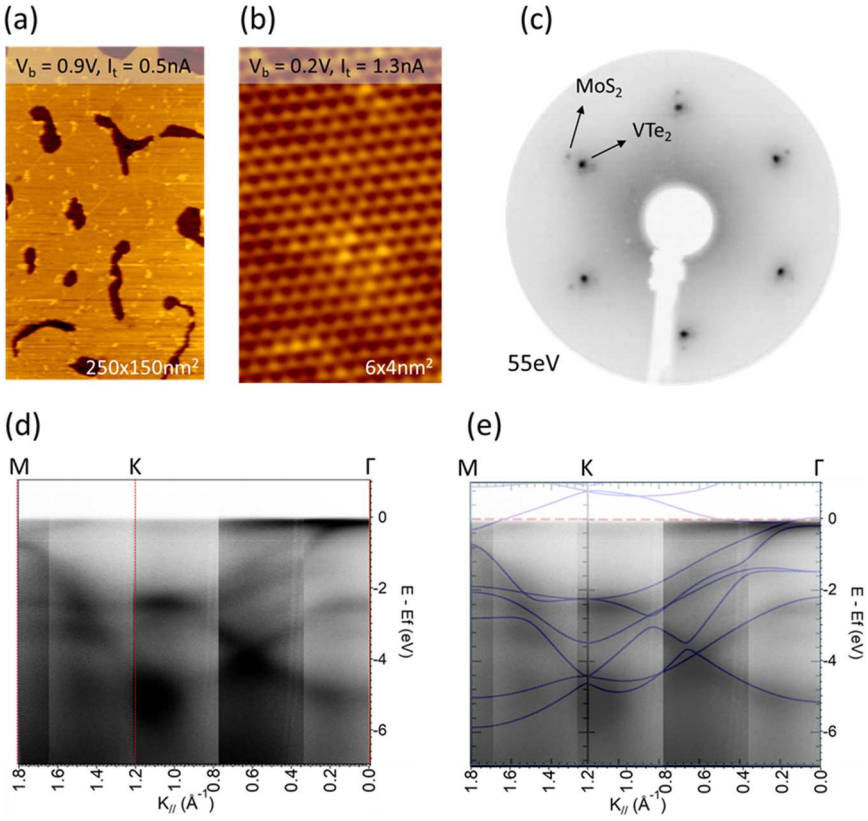

Figure 2. Characterization of monolayer VTe_2. VTe_2 grows in a layer fashion with completion of an almost full monolayer before the second layer nucleates. A large scale STM image of an almost complete monolayer is shown in panel a. Atomic resolution of a simple hexagonal lattice is shown in panel b, while panel c shows the diffraction pattern with both the diffraction spots of the VTe_2 monolayer as well as diffraction spots from the MoS_2 substrate visible. ARPES measurements of a VTe_2 monolayer on the G/SiC substrate are shown in panel d along the Γ−K−M direction. Comparison to DFT band structure calculations for a 1T-VTe_2 monolayer shows close agreement with the measurements, indicating that the film is indeed 1T VTe_2. The DFT band structure and ARPES spectra are overlaid in panel e.

orbitals above the Fermi level and thus causing a charge transfer from the occupied tellurium states to the vanadium 3d orbitals.[17] Consequently, interlayer couplings control the d electron count, and thus, structural control may be asserted by modifying interlayer interactions. Specifically, here we show that the absence of interlayer coupling in monolayers leads to a lifting of the structural distortion and formation of a simple 1T structure in contrast to the 1T′ structure for multilayer samples. In this novel 1T form of VTe_2, a 4 × 4 CDW is observed that is unique to the monolayer. The layer dependence of CDW transitions has been a central aspect in gaining a better understanding in the origins of CDW in TMDCs.[18−29] Generally, in these studies, a preservation of the CDW properties of the bulk down to the monolayer is observed with only some variations in transition temperatures. The coupling of the CDW to the layer-dependent structural transition sets VTe_2 apart from all of the other TMDC materials and enables the CDW behavior to be restricted to the monolayer limit.

Figure 1 shows scanning tunneling microscope (STM) imaging and low-energy electron diffraction (LEED) of multilayer samples (approximately two to three layers). The

DOI: 10.1021/acs.jpclett.9b01949
J. Phys. Chem. Lett. 2019, 10, 4987−4993

STM image reveals that these multilayer samples expose regions with different numbers of layers given a terraced surface morphology. In higher-resolution images, structural domains are observed with three equivalent rotational domains. Atomic resolution shows that the structure can be described by a 2 × 1 unit cell with respect to the hexagonal lattice. Three rotational domains with a 2 × 1 periodicity are also consistent with the LEED pattern, shown in Figure 1d. The formation of a 2 × 1 periodicity in multilayer samples is different from what would be expected of bulk surfaces of group V tellurides that are reported to exhibit 3 × 1 structures,[15] consistent with the ribbon structure of these materials. The observed 2 × 1 structure is consistent with a zigzag 1T′ structure and thus suggests that the MBE-grown multilayer VTe_2 exhibits a structure different from that of bulk samples. The same structures are observed for films grown on HOPG, graphene/SiC, or MoS_2, so that substrate effects on the structure seem unlikely.

A structural modification occurs if the film thickness is reduced to a single layer. Figure 2 shows STM images of an almost complete monolayer, which grows perfectly without nucleation of second layers. Atomic-resolution images show that the structure is a simple hexagonal structure, consistent with a 1T structure. The LEED pattern also exhibits a hexagonal structure. In addition to the LEED spots originating from the VTe_2 monolayer, the diffraction spots from the MoS_2 substrates are also identified. Using the known lattice constant of MoS_2 (a_{MoS_2} = 0.316 nm), we measure a lattice constant for VTe_2 (a_{VTe_2}) of 0.36 nm, which is close to the expected lattice constant for bulk VTe_2, indicating that VTe_2 grows unstrained by van der Waals epitaxy on these substrates. To confirm that the structure is 1T VTe_2, we performed ARPES on a VTe_2 monolayer grown on a bilayer graphene/SiC substrate along the Γ−K−M direction and compared it to electronic structure calculations by density functional theory (DFT). Although the graphene is single-crystalline, the grown VTe_2 is not in perfect epitaxial relationship, as the LEED pattern shown in Figure S1 shows. Nevertheless, the preferential alignment is sufficient to obtain good quality ARPES data, consistent with other ARPES studies of such van der Waals systems. The measured band structure for VTe_2 is in good agreement with the calculated band structure for 1T VTe_2 as shown in Figure 2, thus verifying the crystal structure of the monolayer. Close to the Γ point, a strong V-derived flat band is observed close to the Fermi level that turns above the Fermi level at around the halfway point in the Γ−K direction. Two Te 5p-derived hole pockets are close to the Fermi level at the Γ point and disperse downward in the Γ−K direction. At the M point, the V 3d band forms an electron pocket. In addition to VTe_2 on graphene/SiC, we also performed ARPES of VTe_2/MoS_2 samples, shown in Figure S1. The presence of the MoS_2 substrate makes an identification of the VTe_2 bands more challenging, but the same band structure for VTe_2 can be identified, indicating that we are growing the same 1T phase on both substrates.

To explore the structural stability of these phases of VTe_2, we performed phonon-dispersion calculations by DFT using LDA. Panels a and b of Figure 3 show that while the 1T′ phase is stable, the 1T phase exhibits negative frequencies indicative of imaginary phonon modes. Such a phonon instability of the 1T phase is suggestive of a CDW transition. The negative modes appear around halfway between Γ−M in the Brillouin

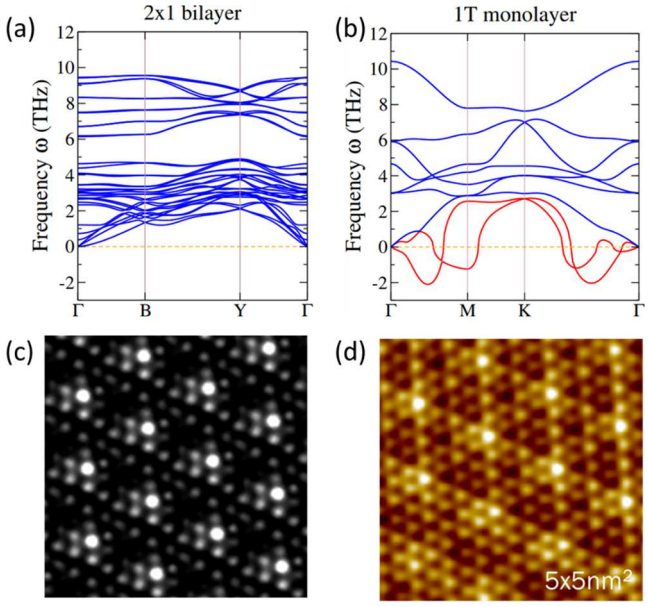

Figure 3. Charge density wave instability in monolayer 1T VTe_2. Calculated phonon dispersions are shown for (a) the 1T′ phase and (b) the 1T monolayer. The 1T phase exhibits negative frequencies at half-distance between Γ and M indicating a dynamic instability of the 1T monolayer with a 4 × 4 periodicity. The simulated STM image of a 4 × 4 CDW is shown in panel c, and the experimentally determined 4 × 4 CDW reconstruction via scanning tunneling microscopy at 20 K is shown in panel d.

zone. Using a zone folding scheme of a 4 × 4 structure, we can show that all of the imaginary modes fold back onto the Γ point demonstrating a 4 × 4 CDW unit cell (see Figure S2). The prediction of a CDW instability is confirmed by the STM at 20 K, which shows a clear 4 × 4 superstructure. To determine the crystal structure of the CDW phase, atoms of a 4 × 4 superstructure are displaced along the eigenvector of the negative mode mentioned above. After relaxing the displaced structures, we obtain a distorted phase, whose energy is 20 meV/atom lower than that of the perfect 1T structure. Calculated phonon dispersion of 4 × 4 CDW structure indicates that it is dynamically stable (see Figure S3). Using a Tersoff−Hamann approach,[30] the STM image of this CDW structure is simulated and compared with the experiment. Good agreement is obtained as is seen from comparing panels c and d of Figure 3. It is noteworthy that we do not find any evidence of a CDW in the STM image for the multilayer 1T′ samples. This seems to contradict recent reports that observed resistance changes in transport measurements that were attributed to CDW transitions in MBE-grown multilayer VTe_2 samples.[31] While sample growth is similar, the reported transport measurements were, however, performed on air-exposed samples, which causes uncontrolled adsorption that may change the material property. In this context, it may be noteworthy that our monolayer and few-layer samples are unstable in air. X-ray photoemission spectroscopy (XPS) shows strong oxidation of both V and Te after exposure to air, and good-resolution scanning tunneling microscopy is not possible anymore.

Experimental evidence that the observed layer-dependent structural transition in VTe_2 can be attributed to Te to V charge redistribution as a consequence of interlayer interactions comes from photoemission studies. While several

DOI: 10.1021/acs.jpclett.9b01949
J. Phys. Chem. Lett. 2019, 10, 4987−4993

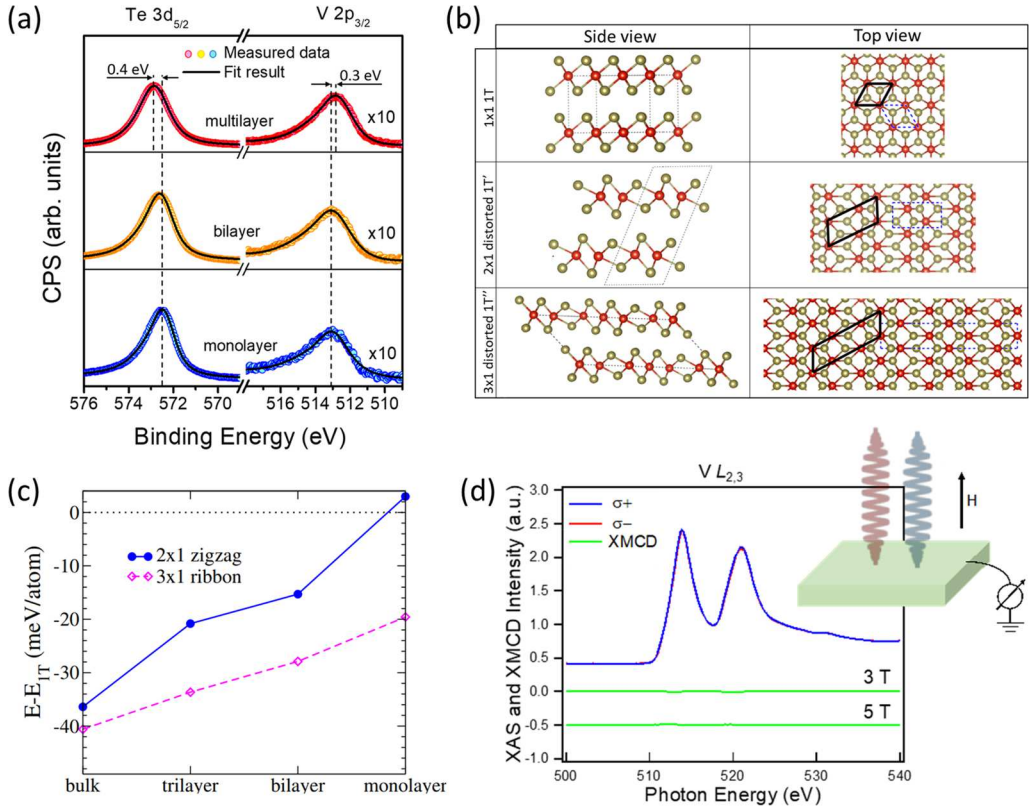

Figure 4. Layer-dependent property variations of VTe_2. The core level shift of Te 3d to a higher binding energy and V 2p to a lower binding energy with an increase in the number of layers is shown in panel a. Ball-and-stick models of the three different structures of VTe_2 are illustrated in panel b, with the top view showing only atoms of a single van der Waals layer. Formation energies for the zigzag 2 × 1 and ribbon 3 × 1 1T′ structures relative to the formation energies of the 1T structure are plotted in panel c as a function of layer thickness. With a decrease in layer thickness, the difference in energy between the structures decreases. X-ray absorption (XAS) of the V $L_{2,3}$ edge and the XMCD signal for an applied field of 3 and 5 T are shown in panel d. The absence of any XMCD signal suggests that VTe_2 is nonmagnetic.

effects that occur simultaneously such as splitting of energy levels due to changed crystal fields, changing unit cells, and shifting of energy levels make it challenging to directly compare ARPES data for monolayer and few-layer samples of a 1T and 1T′ phase, we instead investigate core level binding energy shifts by XPS. Figure 4a shows the Te $3d_{5/2}$ and V $2p_{3/2}$ peak for different layer thicknesses (the full Te 3d and V 2p spectra are shown in Figure S4). The Te peak shifts by ∼0.4 eV to a higher binding energy for thicker films compared to the monolayer, while the V 2p peak shifts in the opposite direction by ∼0.3 eV to a lower binding energy. This indicates a less negative charge state of Te in the multilayer and thus charge transfer from Te to V. While such charge transfer may explain the 1T structure for the monolayer, the 1T′ phase is usually expected for an even higher d electron count than the ribbon structure;[16] i.e., within this charge transfer model, an enhanced charge transfer for multilayers is implied compared to bulk samples. Currently, we cannot conclusively explain why the zigzag 1T′ should be favored over the ribbon 1T′ structure for multilayers. However, it is interesting to point out that for the related $TiTe_2$ system a reduced *c* lattice constant compared to bulk values for MBE-grown multilayer samples was recently reported.[32] This would suggest stronger interlayer Te−Te contacts and thus enhanced charge transfer. If a similar decrease in the interlayer gap occurs in VTe_2, this could explain the formation of the 1T′ structure.

A comparison of the formation energies in DFT calculations also shows that the energy differences among the three structures become smaller as the film thickness is reduced. Figure 4c shows the formation energy of the two ribbon structures, i.e., zigzag (2 × 1) and ribbon (3 × 1), as a function of the number of layers relative to the 1T structure. Consistent with our observations the 1T structure becomes favored over the 2 × 1 structure only for the monolayer. Similarly, the difference in energy between the 1T form and the 3 × 1 form continues to decrease with a decreasing number of layers, but the 3 × 1 structure remains the lowest-energy configuration among those polymorphs even for the monolayer. It is important to point out, though, that as we mentioned above the 4 × 4 CDW in the monolayer lowers the 1T structure by ∼20 meV/atom and thus makes the 1T structure comparable in energy to the 3 × 1 structure. While this could explain the stability of the 1T structure even in 0 K calculations, we may also consider that all samples were grown at ∼600 K, at which anharmonicity is significant, and this may favor the 2 × 1 structures for the multilayer and 1T for the monolayer structure. Upon cooling, monolayer 1T experiences spontaneous breaking of symmetry and transforms to the energy-lowering CDW structure. It is noticed that no soft modes at any commensurate q point support a transition to the 3 × 1 structure in the monolayer limit. Meanwhile, multilayer 2 × 1 structures are metastable at a local minimum of the potential energy surface, and kinetic barriers may prevent transformation to the lower-energy 3 × 1 structure at low temperatures. In general, the DFT calculations show that the energy differences of the three structures are subtle in the monolayer and this may

DOI: 10.1021/acs.jpclett.9b01949
J. Phys. Chem. Lett. 2019, 10, 4987−4993

allow the structure to be controlled, especially by tuning interlayer interactions in van der Waals heterostructures.

Magnetic ordering in monolayer vanadium dichalcogenides has been a contentious topic,[25−28,33,34] and VTe_2 has also been suggested from DFT to exhibit ferromagnetic ordering in the monolayer limit.[35,36] We determine the absence of magnetic ordering of our VTe_2 samples by X-ray magnetic circular dichroism (XMCD). Typical XAS and XMCD spectra of VTe_2, normalized to the incident beam intensity, are presented in Figure 4d. The XAS spectra of V for both left- and right-circularly polarized X-rays show a wide line at each spin−orbit split core level without prominent multiplet structure. This is proof that the sample has been well protected from oxidation by the Te-capping layer. No appreciable XMCD was detected in applied magnetic fields of either 3 or 5 T, suggesting no intrinsic magnetism of the VTe_2 monolayer.

In conclusion, a new CDW material in the form of 1T VTe_2 has been discovered. The 1T phase of VTe_2 is stable only in the monolayer limit, suggesting that interlayer interactions in multilayer and bulk VTe_2 are responsible for the distortion of the 1T structure into 1T′ phases. This demonstrates that tuning of the interlayer interactions, in, for example, van der Waals heterostructures, can be used not only to control electronic properties but also to induce structural variations and tune many-body physics phenomena like CDW transitions.

METHODS

To study the layer-dependent properties in VTe_2, we grew films by molecular beam epitaxy (MBE) on different van der Waals substrates, namely, graphite/HOPG, bilayer graphene/6H-SiC, and MoS_2 single crystals. The substrates are cleaved in air and outgassed in UHV at 300 °C for 2 h, prior to growth. V is evaporated from a mini e-beam evaporator, while Te is co-deposited from a K-cell. The Te flux exceeds the V flux by a factor of ∼10. The optimum growth temperature was established to be ∼300 °C with a growth rate of one monolayer (ML) in ∼16 min. The grown samples were transferred in situ from the growth chamber to a surface analysis chamber equipped with a Scienta R3000 hemispherical analyzer for photoemission spectroscopy, LEED, and a room-temperature STM. For angle-resolved photoemission, a refocused VUV He-discharge lamp using the He−I line was used and the measurements were taken with the sample at room temperature. X-ray photoemission was conducted using a dual-anode X-ray source, and the spectra shown here used nonmonochromatized Al Kα radiation. Additional characterization was performed in a variable-temperature (VT) STM with a lowest temperature of 20 K. For these studies, the sample was transferred in a vacuum suitcase from the growth chamber to the VT STM. In addition, magnetic characterization by XMCD of the V $L_{2,3}$ absorption edges was performed at beamline I10 of the Diamond Light Source in the United Kingdom. For these measurements, the MBE-grown VTe_2 samples were capped with an ∼10 nm Te capping layer and shipped in an inert gas atmosphere to the United Kingdom. XMCD measurements were obtained by using ∼100% circularly polarized X-rays with normal incidence with respect to the sample plane and parallel to the applied magnetic field, that is, in Faraday geometry. XAS measurements were carried out at 300 K using total electron yield (TEY) detection. XMCD was obtained by taking the difference of the XAS spectra, $\sigma_- - \sigma_+$, obtained by flipping the X-ray helicity at a fixed magnetic field up to 50 kOe. DFT for geometry optimization and electronic structure calculations were performed using the Vienna Ab-initio Simulation Package (VASP).[41] Projector augmented wave (PAW)[42] pseudopotentials and a local density approximation (LDA) functional with a 500 eV plane wave energy cutoff were used. Brillouin zones of 1T, 2 × 1, and 3 × 1 structures were sampled with dense k-point 11 × 11, 5 × 11, and 3 × 9 grids, respectively. Crystal structure optimization was performed with a force tolerance of 0.001 eV/Å.

ASSOCIATED CONTENT

Supporting Information

The Supporting Information is available free of charge on the ACS Publications website at DOI: 10.1021/acs.jpclett.9b01949.

Comparison of LEED and ARPES of monolayer VTe_2 on different van der Waals substrates, zone folding and phonon dispersion of 4 × 4 CDW in monolayer VTe_2, and XPS spectra of Te 3d and V 2p as a function of the number of layers (PDF)

AUTHOR INFORMATION

Corresponding Author

*E-mail: mbatzill@usf.edu.

ORCID

Ivan I. Oleynik: 0000-0002-5348-6484

Matthias Batzill: 0000-0001-8984-8427

Author Contributions

P.M.C. and K.L. grew the samples and characterized them via RT-STM, XPS, and ARPES experiments. K.N.C. and I.I.O. performed DFT calculations. J.L. performed LT-STM studies. W.N. and W.L. performed synchrotron XAS and XMCD studies. M.B. directed the research and wrote the manuscript. All authors contributed to the analysis, discussion, and presentation of the data.

Notes

The authors declare no competing financial interest.

ACKNOWLEDGMENTS

Financial support from the National Science Foundation via Grants DMR-1701390 and CHE-1801199 is acknowledged. W.N. and W.L. acknowledge support by UK EPSRC EP/S010246/1, Royal Society IEC\NSFC\181680, and Leverhulme Trust LTSRF1819\15\12. The Diamond Light source is acknowledged under Proposal MM22532.

REFERENCES

(1) Mak, K. F.; Lee, C.; Hone, J.; Shan, J.; Heinz, T. F. Atomically Thin MoS_2: A New Direct-Gap Semiconductor. *Phys. Rev. Lett.* **2010**, *105*, 136805.

(2) Cheng, Y.; Zhu, Z.; Schwingenschlögl, U. Role of Interlayer Coupling in Ultra Thin MoS_2. *RSC Adv.* **2012**, *2*, 7798−7802.

(3) Klein, A.; Tiefenbacher, S.; Eyert, V.; Pettenkofer, C.; Jaegermann, W. Electronic Band Structure of Single-Crystal and Single-Layer WS_2: Influence of Interlayer Van der Waals Interactions. *Phys. Rev. B: Condens. Matter Mater. Phys.* **2001**, *64*, 205416.

(4) Wang, Y.; Li, L.; Yao, W.; Song, S.; Sun, J. T.; Pan, J.; Ren, X.; Li, C.; Okunishi, E.; Wang, Y.-Q.; et al. Monolayer $PtSe_2$, a New Semiconducting Transition-Metal-Dichalcogenide, Epitaxially Grown by Direct Selenization of Pt. *Nano Lett.* **2015**, *15*, 4013−4018.

DOI: 10.1021/acs.jpclett.9b01949
J. Phys. Chem. Lett. 2019, 10, 4987−4993

(5) Ciarrocchi, A.; Avsar, A.; Ovchinnikov, D.; Kis, A. Thickness-Modulated Metal-to-Semiconductor Transformation in a Transition Metal Dichalcogenide. *Nat. Commun.* **2018**, *9*, 919.
(6) Zhao, Y.; Qiao, J.; Yu, P.; Hu, Z.; Lin, Z.; Lau, S. P.; Liu, Z.; Ji, W.; Chai, Y. Extraordinarily Strong Interlayer Interaction in 2D Layered PtS_2. *Adv. Mater.* **2016**, *28*, 2399−2407.
(7) Chen, P.; Chan, Y.-H.; Fang, X.-Y.; Zhang, Y.; Chou, M. Y.; Mo, S.-K.; Hussain, Z.; Fedorov, A.-V.; Chiang, T.-C. Charge Density Wave Transition in Single-Layer Titanium Diselenide. *Nat. Commun.* **2015**, *6*, 8943.
(8) Kolekar, S.; Bonilla, M.; Diaz, H. C.; Hashimoto, M.; Lu, D.; Batzill, M. Controlling the Charge Density Wave Transition in Monolayer $TiSe_2$: Substrate and Doping Effects. *Adv. Quantum Technol.* **2018**, *1*, 1800070.
(9) Chen, P.; Pai, W. W.; Chan, Y.-H.; Takayama, A.; Xu, C.-Z.; Karn, A.; Hasegawa, S.; Chou, M. Y.; Mo, S.-K.; Fedorov, A.-V.; Chiang, T.-C. Emergence of Charge Density Waves and a Pseudogap in Single-Layer $TiTe_2$. *Nat. Commun.* **2017**, *8*, 516.
(10) Chen, Y.; Ruan, W.; Wu, M.; Tang, S.; Ryu, H.; Tsai, H.-Z.; Lee, R.; Kahn, S.; Liou, F.; Jia, C. Visualizing Exotic Orbital Texture in the Single-Layer Mott Insulator 1T-$TaSe_2$. *arXiv* **2019**, 1904.11010.
(11) Chen, C.; Kim, H.-S.; Admasu, A. S.; Cheong, S.-W.; Haule, K.; Vanderbilt, D.; Wu, W. Trimer Bonding States on the Surface of the Transition-Metal Dichalcogenide $TaTe_2$. *Phys. Rev. B: Condens. Matter Mater. Phys.* **2018**, *98*, 195423.
(12) Chen, H.; Li, Z.; Fan, X.; Guo, L.; Chen, X. Quantum Linear Magnetoresistance in $NbTe_2$. *Solid State Commun.* **2018**, *275*, 16−20.
(13) Sörgel, T.; Nuss, J.; Wedig, U.; Kremer, R. K.; Jansen, M. A New Low Temperature Modification of $TaTe_2$—Comparison to the Room Temperature and the Hypothetical 1T-$TaTe_2$ Modification. *Mater. Res. Bull.* **2006**, *41*, 987−1000.
(14) Bronsema, K. D.; Bus, G. W.; Wiegers, G. A. The Crystal Structure of Vanadium Ditelluride, $V_{1+x}Te_2$. *J. Solid State Chem.* **1984**, *53*, 415−421.
(15) Kim, S.-J.; Park, S.-J.; Oh, H.-J.; Jeon, I. C.; Song, S. Atomic Force Microscopy Study of Conducting Layered Transition Metal Ditelluride. *Bull. Korean Chem. Soc.* **1994**, *15*, 1098−1103.
(16) Whangbo, M.-H.; Canadell, E. Analogies between the Concepts of Molecular Chemistry and Solid-State Physics concerning Structural Instabilities. Electronic Origin of the Structural Modulations in Layered Transition-Metal Dichalcogenides. *J. Am. Chem. Soc.* **1992**, *114*, 9587−9600.
(17) Canadell, E.; Jobic, S.; Brec, R.; Rouxel, J.; Whangbo, M.-H. Importance of Short Interlayer Te-Te Contacts for the Structural Distortions and Physical Properties of CdI_2-Type Layered Transition-Metal Ditellurides. *J. Solid State Chem.* **1992**, *99*, 189−199.
(18) Rossnagel, K. On the Origin of Charge-Density Waves in Select Layered Transition-Metal Dichalcogenides. *J. Phys.: Condens. Matter* **2011**, *23*, 213001.
(19) Zhu, X.; Cao, Y.; Zhang, J.; Plummer, E. W.; Guo, J. Classification of Charge Density Waves Based on their Nature. *Proc. Natl. Acad. Sci. U. S. A.* **2015**, *112*, 2367−2371.
(20) Zhang, Z. P.; Yang, P. F.; Hong, M.; Jiang, S. L.; Zhao, G. C.; Shi, J. P.; Xie, Q.; Zhang, Y. F. Recent Progress in the Controlled Synthesis of 2D Metallic Transition Metal Dichalcogenides. *Nanotechnology* **2019**, *30*, 182002.
(21) Manzeli, S.; Ovchinnikov, D.; Pasquier, D.; Yazyev, O. V.; Kis, A. 2D Transition Metal Dichalcogenides. *Nat. Rev. Mater.* **2017**, *2*, 17033.
(22) Xi, X.; Zhao, L.; Wang, Z.; Berger, H.; Forro, L.; Shan, J.; Mak, K. F. Strongly Enhanced Charge-Density-Wave Order in Monolayer $NbSe_2$. *Nat. Nanotechnol.* **2015**, *10*, 765−769.
(23) Ugeda, M. M.; Bradley, A. J.; Zhang, Y.; Onishi, S.; Chen, Y.; Ruan, W.; Ojeda-Aristizabal, C.; Ryu, H.; Edmonds, M. T.; Tsai, H.-Z.; et al. Characterization of Collective Ground States in Single-Layer $NbSe_2$. *Nat. Phys.* **2016**, *12*, 92−98.
(24) Kolekar, S.; Bonilla, M.; Ma, Y.; Diaz, H. C.; Batzill, M. Layer- and Substrate-Dependent Charge Density Wave Criticality in 1T−$TiSe_2$. *2D Mater.* **2018**, *5*, 015006.
(25) Coelho, P.; Nguyen Cong, K.; Bonilla, M.; Kolekar, S.; Phan, M.-H.; Avila, J.; Asensio, M. C.; Oleynik, I. I.; Batzill, M. Charge Density Wave State Suppresses Ferromagnetic Ordering in VSe_2 Monolayers. *J. Phys. Chem. C* **2019**, *123*, 14089−14096.
(26) Chen, P.; Pai, W. W.; Chan, Y.-H.; Madhavan, V.; Chou, M. Y.; Mo, S.-K.; Fedorov, A.-V.; Chiang, T.-C. Unique Gap Structure and Symmetry of the Charge Density Wave in Single-Layer VSe_2. *Phys. Rev. Lett.* **2018**, *121*, 196402.
(27) Duvjir, G.; Choi, B. K.; Jang, I.; Ulstrup, S.; Kang, S.; Thi Ly, T.; Kim, S.; Choi, Y. H.; Jozwiak, C.; Bostwick, A.; et al. Emergence of a Metal−Insulator Transition and High-Temperature Charge-Density Waves in VSe_2 at the Monolayer Limit. *Nano Lett.* **2018**, *18*, 5432−5438.
(28) Feng, J.; Biswas, D.; Rajan, A.; Watson, M. D.; Mazzola, F.; Clark, O. J.; Underwood, K.; Marković, I.; McLaren, M.; Hunter, A.; et al. Electronic Structure and Enhanced Charge-Density Wave Order of Monolayer VSe_2. *Nano Lett.* **2018**, *18*, 4493−4499.
(29) Ryu, H.; Chen, Y.; Kim, H.; Tsai, H.-Z.; Tang, S.; Jiang, J.; Liou, F.; Kahn, S.; Jia, C.; Omrani, A. A.; et al. Persistent Charge-Density-Wave Order in Single-Layer $TaSe_2$. *Nano Lett.* **2018**, *18*, 689−694.
(30) Tersoff, J.; Hamann, D. R. Theory and Application for the Scanning Tunneling Microscope. *Phys. Rev. Lett.* **1983**, *50*, 1998−2001.
(31) Ma, X.; Dai, T.; Dang, S.; Kang, S.; Chen, X.; Zhou, W.; Wang, G.; Li, H.; Hu, P.; He, Z.; et al. Charge Density Wave Phase Transitions in Large-Scale Few-Layer 1T-VTe_2 Grown by Molecular Beam Epitaxy. *ACS Appl. Mater. Interfaces* **2019**, *11*, 10729−10735.
(32) Fragkos, S.; Sant, R.; Alvarez, C.; Bosak, A.; Tsipas, P.; Tsoutsou, D.; Okuno, H.; Renaud, G.; Dimoulas, A. Room Temperature Commensurate Charge Density Wave in Epitaxial Strained $TiTe_2$ Multilayer Films. *Adv. Mater. Interfaces* **2019**, *6*, 1801850.
(33) Ma, Y.; Dai, Y.; Guo, M.; Niu, C.; Zhu, Y.; Huang, B. Evidence of the Existence of Magnetism in Pristine VX_2 Monolayers (X = S, Se) and Their Strain-Induced Tunable Magnetic Properties. *ACS Nano* **2012**, *6*, 1695−1701.
(34) Bonilla, M.; Kolekar, S.; Ma, Y.; Coy Diaz, H.; Kalappattil, V.; Das, R.; Eggers, T.; Gutierrez, H. R.; Phan, M.-H.; Batzill, M. Strong Room-Temperature Ferromagnetism in VSe_2 Monolayers on Van der Waals Substrates. *Nat. Nanotechnol.* **2018**, *13*, 289−293.
(35) Pan, H. Magnetic and Electronic Evolutions of Hydrogenated VTe_2 Monolayer under Tension. *Sci. Rep.* **2015**, *4*, 7524.
(36) Fuh, H.-R.; Chang, C.-R.; Wang, Y.-K.; Evans, R. F. L.; Chantrell, R. W.; Jeng, H.-T. New Type Single-Layer Magnetic Semiconductor in Transition-Metal Dichalcogenides VX_2 (X = S, Se and Te). *Sci. Rep.* **2016**, *6*, 32625.
(37) Wong, P. K. J.; Zhang, W.; Zhou, J.; Bussolotti, F.; Yin, X.; Zhang, L.; N'Diaye, A. T.; Morton, S. A.; Chen, W.; Goh, K. E. J. Evidence for Metallic 1T phase, $3d^1$ Electronic Configuration and Charge Density Wave Order in Molecular-Beam Epitaxy Grown Monolayer VTe_2. *arXiv* **2019**, 1907.06185.
(38) Miao, G.; Xue, S.; Li, B.; Lin, Z.; Liu, B.; Zhu, X.; Wang, W.; Guo, J. Real-Space Investigation of the Charge Density Wave in VTe_2 Monolayer with Rotational and Mirror Symmetries Broken. *arXiv* **2019**, 1908.00714.
(39) Sugawara, K.; Nakata, Y.; Fujii, K.; Nakayama, K.; Souma, S.; Takahashi, T.; Sato, T. Monolayer VTe_2: Incommensurate Fermi Surface Nesting and Suppression of Charge Density Waves. *arXiv* **2019**, 1906.07855.
(40) Wang, Y.; Ren, J.; Li, J.; Wang, Y.; Peng, H.; Yu, P.; Duan, W.; Zhou, S. Evidence of Charge Density Wave with Anisotropic Gap in Monolayer VTe_2 Film. *arXiv* **2019**, 1905.13446.
(41) Kresse, G.; Furthmüller, J. Efficiency of Ab-Initio Total Energy Calculations for Metals and Semiconductors Using a Plane-Wave Basis Set. *Comput. Mater. Sci.* **1996**, *6*, 15−50.
(42) Blöchl, P. E. Projector Augmented Wave Method. *Phys. Rev. B: Condens. Matter Mater. Phys.* **1994**, *50*, 17953−17979.

DOI: 10.1021/acs.jpclett.9b01949
J. Phys. Chem. Lett. 2019, 10, 4987−4993

NOTE ADDED IN PROOF

During final submission of the manuscript, we became aware of manuscripts[37−40] that are consistent with our observation of a 4 × 4 CDW in monolayer VTe_2.

DOI: 10.1021/acs.jpclett.9b01949
J. Phys. Chem. Lett. 2019, 10, 4987−4993